Power Engineering and Engineering Thermophysics
https://www.acadlore.com/journals/PEET

Diffusion Characteristics of Combustible Gas Leaks in the FPSO Upper Module

Longting Wang[1], Yaonan Wu[2*], Zhen Long[1], Zimo Liu[3], Zhihui Liu[4], Zhang Shi[1], Yanqun Yu[1]

[1] College of Mechanical and Electronic Engineering, China University of Petroleum (East China), 266580 Qingdao, China
[2] CNNC No. 7 Research & Design Institute Co., Ltd., 030200 Taiyuan, China
[3] Faculty of Built Environment, University of Malaya, 50603 Kuala Lumpur, Malaysia
[4] School of Petroleum Engineering, China University of Petroleum (East China), 266580 Qingdao, China

* Correspondence: Yaonan Wu (wuyaonan@cnsi.ltd)

Received: 07-28-2024 **Revised:** 09-06-2024 **Accepted:** 09-13-2024

Citation: L. T. Wang, Y. N. Wu, Z. Long, Z. M. Liu, Z. H. Liu, Z. Shi, and Y. Q. Yu, "Diffusion characteristics of combustible gas leaks in the FPSO upper module," *Power Eng. Eng. Thermophys.*, vol. 3, no. 3, pp. 158–175, 2024. https://doi.org/10.56578/peet030302.

Abstract: To investigate the variation in the diffusion patterns of natural gas leaks in the Floating Production Storage and Offloading (FPSO) system, with the aim of formulating appropriate emergency response strategies and minimizing accident losses, a study was conducted on the gas leak issues of oil and gas processing equipment in the FPSO upper module. A consequence prediction and assessment model was established based on Computational Fluid Dynamics (CFD) methods. Sixteen working conditions and one control working condition were developed to simulate the diffusion characteristics of combustible gas leaks. The simulations provided insights into the gas leakage patterns under different conditions and identified the most hazardous scenario for gas leaks in the FPSO upper module. The results indicate that the density and shape of the equipment within the upper module significantly influence the diffusion outcome. After a leak, high concentrations of combustible gas were observed near the crude oil heat exchanger skid in Industrial Zone II. The effects of individual factors on gas diffusion were significant, and the interactions among multiple factors were complex. Wind speed had a more pronounced effect on longitudinal gas diffusion compared to wind direction and leak aperture, while wind direction significantly influenced lateral gas diffusion. The leak aperture, on the other hand, had a more substantial impact on vertical gas diffusion.

Keywords: Floating production storage and offloading; Oil and gas processing system; Natural gas leak; Consequence simulation; Diffusion characteristics

1 Introduction

Driven by increasing energy demands, oil and gas extraction has progressively shifted from land to offshore environments, with a significant rise in offshore oil and gas production in recent years [1]. The primary risks associated with offshore oil and gas development arise from facility defects and human errors that lead to oil and gas leaks. Over 70% of offshore platform accidents are attributed to gas leaks caused by operational errors, equipment malfunctions, and management deficiencies. During the oil and gas processing stages on offshore platforms, leaks involving natural gas and hydrocarbon gases present a high risk of causing explosions or fires [2–6], potentially resulting in significant loss of life and severe damage to equipment. The FPSO system is a multifunctional, large-scale offshore platform that integrates oil and gas processing, storage and offloading, wastewater treatment, and power generation. Due to the harsh operational environment, the oil and gas processing areas in the upper modules of FPSO are particularly vulnerable to the risk of gas leaks. When gas leaks come into contact with an ignition source, they can lead to fires or explosions, triggering a chain reaction of secondary hazards, including system failure, further leaks, and additional explosions. These events can cause catastrophic casualties and extensive economic losses. It is therefore crucial to conduct a scientific and effective analysis of combustible gas leak diffusion characteristics during the operation of oil and gas facilities. This enables a more accurate understanding of gas diffusion patterns and predictions of potential outcomes following a leak, allowing for timely and effective control measures to prevent subsequent combustible gas cloud explosions.

Numerical simulations and experimental analyses are considered effective tools for analysing the consequences of natural gas diffusion [7, 8]. Researchers have extensively studied gas leaks, diffusion, and fire explosion patterns in FPSO from various perspectives, thereby refining and expanding the research framework for FPSO leak and explosion studies. Explosion and fire engineering of floating, production, storage and off-loading units (EFEF JIP) [9–12] have significantly expanded the knowledge domain about offshore explosion phenomenology. Takahashi and Watanabe [13] proposed the use of 3D modelling, CFD, and finite element simulation techniques to simulate explosions on offshore platforms, yielding more accurate risk analysis results. Dan et al. [14] conducted a quantitative analysis of fire and explosion risks under various hazardous working conditions in the upper module of LNG-FPSO using PHAST software, demonstrating its strong applicability in simulating offshore oil and gas leaks. Yang et al. [15] developed a model for the leakage, combustion, and explosion of toxic gases on offshore platforms and conducted simulations using FLACS software. The simulation results provided significant guidance for the formulation of emergency response plans and the improvement of related safety measures. Liu et al. [16] established a vapour cloud explosion calculation model for offshore platforms using FLACS and validated the model through a series of explosion experiments conducted under the foreign MERGE project. The research indicated that the uniform arrangement of obstacles had the greatest impact. Fang et al. [17] applied FLACS to study the influence of cubic obstacles on shockwave propagation from highly congested FPSO environments. Kang et al. [18] provided a detailed review and analysis of commercial CFD tools to better understand the mechanisms of explosion accidents and to assess explosion risks in offshore facilities. Additionally, Shamsuddin et al. [19] outlined the advantages and disadvantages of using CFD software for gas explosion simulations in the oil and gas processing industry.

Most of the existing studies on the factors affecting combustible gas leak characteristics have been conducted using single-factor controlled variable simulation experiments without a comprehensive multi-factor analysis. Therefore, based on the theoretical model of gas leaks in the FPSO upper module, this study selects appropriate turbulence and diffusion models to investigate the gas flow characteristics and flow field distribution patterns. The possible leakage working conditions were determined according to the actual working environment of the FPSO. On this basis, a simulation model of gas leakage in the upper module of the FPSO was established to study the gas leakage patterns under different working conditions, identify the most hazardous leakage working condition, and provide theoretical data support for future research on gas leak explosions in the FPSO upper module.

2 Theoretical Model of Combustible Gas Leakage in the Upper Module

The flow characteristics of combustible gas after a leak are governed by conservation laws, and the mathematical expressions of these conservation equations are as follows [20, 21]:

$$\frac{\partial \rho}{\partial t} + \nabla \cdot (\rho \vec{v}) = 0 \tag{1}$$

$$\frac{\partial}{\partial t}(\rho \vec{v}) + \nabla \cdot (\rho \vec{v} \vec{v}) = -\nabla p + \nabla \cdot (\bar{\bar{\tau}}) + \rho \vec{g} + \vec{F} \tag{2}$$

$$\frac{\partial}{\partial t}(\rho E) + \nabla \cdot (\vec{v}(\rho E + p)) = \nabla \cdot \left(k_{eff} \nabla T - \sum_i h_i \vec{J}_i \right) \tag{3}$$

where, ρ represents density $\left(\mathrm{kg/m^3}\right)$; t denotes time (s); ∇ is the Laplacian operator; $\vec{v}$ is the velocity vector $(\mathrm{m/s})$; p is pressure (Pa); $\bar{\bar{\tau}}$ represents the stress tensor; $\vec{F}$ is the body force (N); E is the enthalpy of the gas components $(\mathrm{kJ/kg})$; k_{eff} is the effective thermal conductivity, and $\vec{J}_i$ is the heat flux $\left(\mathrm{kW/m^2}\right)$ of component i.

With the continuous improvement of CFD, an increasing number of researchers have begun employing CFD methods to solve fluid-related problems. FLUENT, a risk assessment software in CFD simulation, is characterised by its diverse models and powerful post-processing capabilities, making it highly effective in reproducing fluid dynamics scenarios and ensuring computational accuracy. It has been widely applied in fluid calculations across various fields such as ships, vehicles, railways, and aircraft. Therefore, in this study, FLUENT software was employed to investigate the flow characteristics and diffusion patterns of gas leaks in the FPSO upper module under different independent working conditions.

In FLUENT, fluid flow is classified into two main forms: laminar and turbulent flow. The leakage and diffusion of combustible gases are considered unsteady turbulent movements. The turbulent flow state is highly complex, and the selection of an appropriate turbulence model must consider both the requirements of the computational model and the available computational resources. The commonly used turbulence models in FLUENT for simulating combustible gas flow and diffusion include the Spalart-Allmaras model, the standard $k-\varepsilon$ model, the RNG $k-\varepsilon$ model, the swirl-modified $k-\varepsilon$ model, and the realizable $k-\varepsilon$ model. According to the literature, when obstacles

are present, the realizable $k-\varepsilon$ model provides more accurate simulation results for gas diffusion when compared with experimental data. Therefore, this model was selected for investigating the gas diffusion patterns in this study. The turbulence equations are expressed as follows [22]:

$$\frac{\partial(\rho k)}{\partial t}+\frac{\partial\left(\rho k u_j\right)}{\partial x_j}=\frac{\partial}{\partial x_j}\left[\left(\mu+\frac{\mu_t}{\sigma_k}\right)\frac{\partial k}{\partial x_j}\right]+G_k+G_b-\rho\varepsilon-Y_M+S_k \tag{4}$$

$$\frac{\partial(\rho\varepsilon)}{\partial t}+\frac{\partial\left(\rho\varepsilon u_j\right)}{\partial x_j}=\frac{\partial}{\partial x_j}\left[\left(\mu+\frac{\mu_t}{\sigma_\varepsilon}\right)\frac{\partial\varepsilon}{\partial x_j}\right]+\rho C_1 S_\varepsilon-\rho C_2\frac{\varepsilon^2}{k+\sqrt{v\varepsilon}}+C_{1\varepsilon}\frac{\varepsilon}{k}C_{3\varepsilon}G_b+S_\varepsilon \tag{5}$$

$$C_1=\max\left[0.43,\frac{\eta}{\eta+5}\right] \tag{6}$$

where, k is the turbulent kinetic energy; ε represents the turbulent dissipation rate; σ_k and σ_ε are the turbulent Prandtl numbers for k and ε, with values of 1.0 and 2.0, respectively; x_j and u_j are the coordinates and velocity components; G_k and G_b are the production of turbulent kinetic energy due to mean velocity gradients and buoyancy, respectively; Y_M denotes the contribution of compressible turbulence to overall dissipation; C_2 and $C_{1\varepsilon}$ are constants with default values of 1.9 and 1.44; $C_{3\varepsilon}$ accounts for the effects of buoyancy on ε; S_k and S_ε are source terms that can be defined by the user according to specific requirements.

FLUENT employs the species transport model to address the diffusion of combustible gases. The species transport model includes both a non-reactive species transport model and a finite-rate reaction model. Since the focus of this study is on the diffusion characteristics of combustible gas after leakage, the non-reactive species transport model was selected. The non-reactive species transport model is governed by the conservation law of species, with the corresponding control equation expressed as follows:

$$\frac{\partial}{\partial t}\left(\rho Y_i\right)+\nabla\cdot\left(\rho\vec{v}Y_i\right)=-\nabla\cdot\vec{J_i}+R_i+S_i \tag{7}$$

where, R_i represents the net rate of chemical generation, and S_i denotes the remaining rates.

In summary, FLUENT software was selected to simulate the diffusion phenomena of combustible gas leaks in the upper module of the FPSO. The realizable $k-\varepsilon$ model from the turbulence models and the non-reactive species transport model from the species transport models were employed to calculate the diffusion of combustible gas.

3 Determination of Simulation Working Conditions for Combustible Gas Leakage

The diffusion characteristics of combustible gas following a leak are influenced by the surrounding environment. If the leakage and diffusion characteristics of the FPSO upper module are studied under a single working condition, the complexity of the FPSO's working environment cannot be fully replicated, which may affect the accuracy and effectiveness of the simulation [23]. In this study, the potential gas leakage working conditions of the FPSO upper module were determined based on various factors such as wind direction, wind speed, leakage aperture, and leakage rate, while considering the actual working environment of the FPSO.

(a) Wind direction

The FPSO vessel was used as the primary subject of the study, with the assumption that the wind direction is perpendicular to the vessel. The natural wind directions were set as headwind, tailwind, wind from the port side, and wind from the starboard side.

(b) Wind speed

The FPSO being studied operates in the South China Sea region. According to GB/T28591 *Wind Power Levels* and the principle of the most unfavourable accident conditions, four wind speeds were selected: 0.5 m/s, 4.5 m/s, 8 m/s, and 10 m/s.

A leakage scenario involving the first-stage separator in the upper module of the FPSO was assumed, with the leakage point located at the centre of the inner side of the first-stage separator skid, and the shape of the leakage aperture was assumed to be circular. Following the principle of the most unfavourable accident conditions, the combustible gas was assumed to eject horizontally outward, perpendicular to the side of the first-stage separator. Based on the setup of the FPSO's safety systems, it was assumed that after the detection of the gas leak, the time required to implement emergency shutdown, venting, and ignition control measures was approximately 180 s. Therefore, the leakage duration was set to 180 s.

(c) Leakage aperture and leakage rate

Based on the actual dimensions of the components of the first-stage separator and in accordance with the API RP 579 method for assessing pipeline volumetric defects, four leakage apertures were selected for the FPSO upper module: 40 mm, 60 mm, 80 mm, and 100 mm.

The leakage rate m of the combustible gas is influenced by factors such as the leakage aperture, the pressure inside the equipment container, and the properties of the leaking gas. During the calculation, it is necessary to first determine whether the velocity at the peak point of the outflow has reached the speed of sound. The criteria for this determination is shown as follows:

$$\frac{P_2}{P_1} = \left(\frac{2}{k+1}\right)^{\frac{k}{k-1}} \tag{8}$$

where, P_1 is the pressure inside the leakage aperture (Pa), P_2 is the external pressure (Pa), and k is the heat capacity ratio. The operating pressure of the first-stage separator in this study was set to 2000 KPa, thus P_1 was taken as 2 MPa.

If the ratio on the left side of the equation is greater than that on the right, the velocity at the peak point of the outflow has not reached the speed of sound. The calculation expression for the leakage rate m of the combustible gas is given as follows:

$$m = C_D A P_1 \sqrt{\frac{2M}{R_g T_1} \frac{k}{k-1} \left[\left(\frac{P_2}{P_1}\right)^{2/k} - \left(\frac{P_2}{P_1}\right)^{(k+1)/k}\right]} \tag{9}$$

where, m is the mass flow rate $(\mathrm{kg/s})$, A is the area of the leakage aperture $\left(\mathrm{m}^2\right)$, M is the molar mass of the gas $(\mathrm{kg/mol})$, R_g is the ideal gas constant, taken as $8.314\ \mathrm{J/(mol \cdot K)}$, T_1 is the temperature (K) inside the equipment, and C_D is the discharge coefficient.

If the ratio on the left side of the equation is smaller than that on the right, the velocity at the peak point of the outflow reaches the speed of sound. The calculation for the combustible gas leakage rate m is shown as follows:

$$m = C_D A P_1 \sqrt{\frac{2M}{R_g T_1} \frac{k}{k-1} \left[\left(\frac{P_2}{P_1}\right)^{2/k} - \left(\frac{P_2}{P_1}\right)^{(k+1)/k}\right]} \tag{10}$$

where, the selection of C_D depends on the shape of the leakage aperture. If the aperture is circular, the value is taken as 1; for rectangular or triangular apertures, the values are 0.9 and 0.95, respectively. As the primary component of the leaking gas is methane, the molar mass M is taken as 16.0, and k is set to 1.32. The leakage rates for various leakage apertures, calculated using Eq. (10), are shown in Table 1.

Table 1. Leakage aperture and rate

Leakage Aperture (mm)	Leakage Rate (kg/s)
40	5.188
60	11.334
80	20.752
100	32.425

4 Construction of the Combustible Gas Leakage Simulation Model for the FPSO Upper Module

4.1 Construction of the FPSO Solid Model

In this study, a 3D model was constructed using a 150,000-ton FPSO operating in the South China Sea as a prototype. The FPSO has a length of 250 m, a width of 46 m, and a height of 24.5 m. During the modelling process, factors such as computer performance and the core research focus of the study were considered, and elements such as the operating room, control room, deck stairs, and pipelines were omitted. The upper module equipment was simplified. The model is shown in Figure 1.

In order to simulate the influence of wind fields on the diffusion of combustible gas leaks, an external computational domain was established outside the model, and Boolean operations were applied. When constructing the external computational domain, it was necessary to ensure that the flow field in the outer region was not affected by the ship's structure. After several adjustments, the dimensions of the computational domain were determined as 500 m in length, 200 m in width, and 100 m in height, approximately twice the length, five times the width, and four times the height of the FPSO model. The complete model is shown in Figure 2.

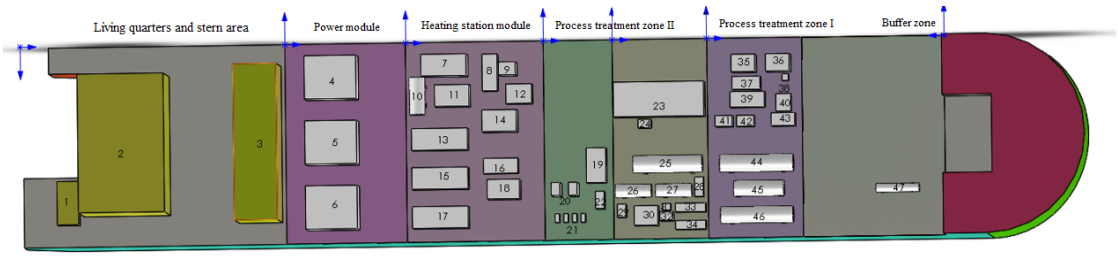

Figure 1. 3D solid model of FPSO

Note: 1- Stern area; 2- Living quarters; 3- Main switch room; 4, 5, 6- Generator room; 7- Inert gas generator; 8- Air compressor; 9- Air bottle; 10- Heat medium expansion tank; 11- Heat medium system oil day-use skid; 12- Nitrogen membrane generator; 13, 15, 17- Heat medium furnace skid; 14- Nitrogen reception device skid; 16- Heat medium circulation pump; 18- Heat medium system oil discharge day-use skid; 19- Fuel oil circulation pump; 20- Qualified oil/diesel booster skid; 21- Fuel oil filter; 22- Crude oil separator skid; 23- Crude oil metering skid; 24- Calibration skid; 25- Electrostatic dehydrator; 26, 27- Crude oil flash skid; 28- Crude oil heat exchanger skid; 29- Electrostatic dehydrator supply skid; 30- Crude oil cooler; 31- Gas cooler; 32- Gas scrubbing skid; 33, 34- Secondary heater; 35, 36- Flotation device skid; 37- Chemical injection skid; 38- Circulating water cooling pump; 39- Chemical agent injection skid; 40- Cooling water circulation pump; 41, 42- Seawater cooler; 43- Cooling water expansion tank skid; 44- Free water separator; 45- First-stage separator; 46- Second-stage separator; 47- Flare liquid separator.

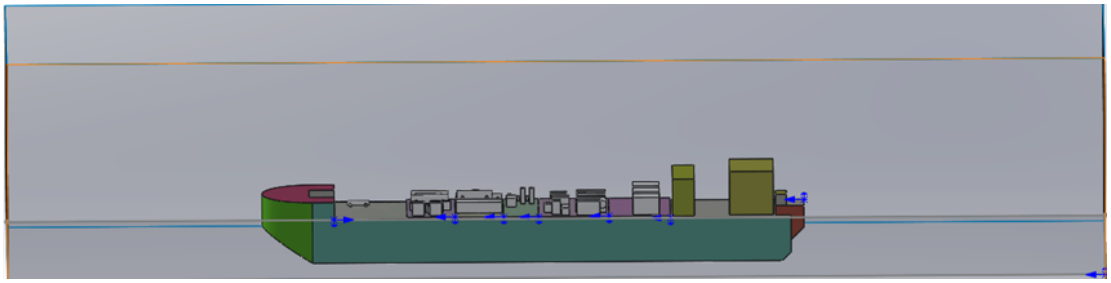

Figure 2. Complete calculation model

4.2 Mesh Generation

Due to the complex structure of the FPSO upper module, it is challenging to apply a hexahedral structured mesh for global meshing, and the calculation results are not ideal. In this study, an unstructured tetrahedral mesh was generated globally for the FPSO using ICEM CFD. Local mesh refinement was applied to the upper module equipment, with density boxes used to refine the mesh around the leakage apertures. Independence tests were conducted to ensure simulation accuracy while reducing computational time and improving efficiency. The results of the mesh generation are shown in Figure 3.

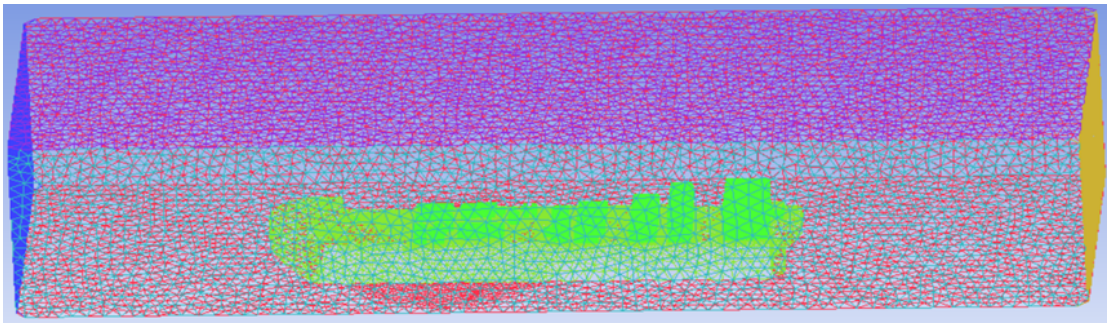

Figure 3. Global meshing results

4.3 Leakage Scenario Setup

Due to the numerous and irregularly arranged structures in the FPSO upper module, the leakage process is exceptionally complex. Therefore, the following assumptions and settings were made for the FPSO gas leakage simulation:

(a) It was assumed that the leaking gas consisted entirely of methane, with an oxygen content of 0.23 in the surrounding air.

(b) The leaking gas was assumed to behave as an incompressible ideal gas throughout the diffusion process.

(c) It was assumed that the gas leaked continuously at a constant mass flow rate, with no heat exchange between the environment and external factors during the diffusion process. The temperature was kept constant at 300K.

(d) The simulation time was set to 180 s, assuming no control measures were taken by personnel during this period, and the combustible gas continued to leak.

(e) Since the density of methane is lower than that of air, the "Full Buoyancy Effects" option was selected in the turbulence model to simulate the buoyancy effects.

4.4 Boundary Condition Setup

When calculating the diffusion of combustible gas leaks using a numerical model, the wind field calculation must first be performed. It was assumed that during the numerical solution process, the fluid variable gradients on the sides and top boundaries of the external domain were set to zero. These boundaries were assigned symmetrical boundary conditions. The inlet wind boundary was set as a velocity inlet, while the outlet was set as a free-flow outlet. All other boundaries were designated as no-slip walls. The simulation was carried out using a steady-state approach. After the convergence criteria were met, the calculation was completed. At this point, the domain was filled with air containing an oxygen content of 0.23.

Once the wind field was stabilised, the species transport model was activated, and the diffusion calculation was performed. During the diffusion calculation, the fuel inlet was set as a mass flow inlet, with the methane composition set to 1. All other settings remained unchanged. A transient calculation was used, with the simulation time set to 180 s.

5 Diffusion Characteristics of Combustible Gas Leaks

The equipment in the upper module of the FPSO is densely arranged. In the event of a combustible gas leak, a flammable gas cloud is likely to form. This could result in a gas cloud explosion, which would generate overpressure and high temperatures, causing casualties and damage to equipment, thus affecting the normal operation of the FPSO. Therefore, studying the diffusion characteristics of combustible gas leaks in the upper module of the FPSO is of practical significance.

5.1 Orthogonal Experimental Design for the Influencing Factors of Combustible Gas Diffusion

The main factors influencing the diffusion characteristics of combustible gas leaks include wind direction, wind speed, and leakage aperture. Each factor can take four variable values, resulting in 64 possible simulation working conditions when combined. The large number of working conditions makes it difficult to simulate gas leaks from the FPSO efficiently. Therefore, an orthogonal experimental design method was adopted to reduce the number of simulations while ensuring results that closely match those obtained from comprehensive experiments. The orthogonal test design for the gas leakage of the FPSO upper module is presented in Table 2.

Table 2. Orthogonal test design for gas leakage in the FPSO upper module

Serial Number	Leakage Aperture (mm)	Leakage Rate (kg/s)	Wind Speed (m/s)	Wind Direction
1	40	5.188	0.5	Headwind
2	60	11.334	4.5	Headwind
3	80	20.752	8	Headwind
4	100	32.425	10	Headwind
5	60	11.334	0.5	Tailwind
6	40	5.188	4.5	Tailwind
7	100	32.425	8	Tailwind
8	80	20.752	10	Tailwind
9	80	20.752	0.5	Port-side wind
10	100	32.425	4.5	Port-side wind
11	60	11.334	10	Port-side wind
12	40	50188	8	Port-side wind
13	100	32.425	0.5	Starboard-side wind
14	60	11.334	4.5	Starboard-side wind
15	60	11.334	8	Starboard-side wind
16	40	5.188	10	Starboard-side wind

5.2 Gas leakage Patterns of the FPSO Upper Module

To explore the impact of influencing factors on the gas leakage patterns of the FPSO, an additional study working condition was introduced based on the orthogonal design. This scenario used a leakage aperture of 40 mm (a commonly used size in offshore analysis) with a corresponding leakage rate of 5.188 kg/s, a wind speed of 4.5 m/s, and headwind conditions as the control group. By comparing the control group with other test scenarios, the effects of different influencing factors on the gas leakage characteristics of the FPSO upper module were investigated.

5.2.1 Wind field and turbulence field

The inlet wind speed was set as the initial condition. After numerical iteration and convergence, a stable wind field was obtained. By establishing a Z=25 plane parallel to the deck, the velocity contour map and the turbulent kinetic energy contour map were generated, as shown in Figure 4.

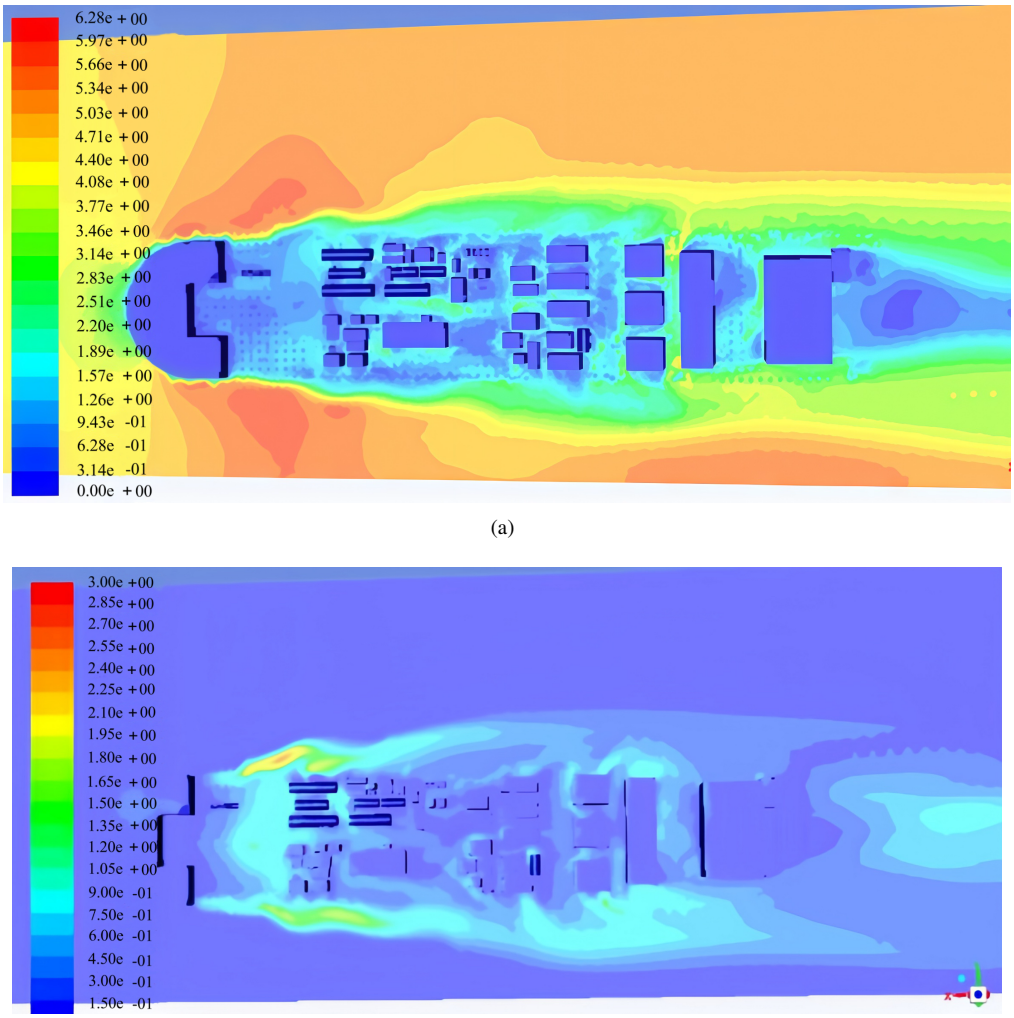

Figure 4. Wind field and turbulence field contour maps of the control group (a) Velocity contour map, (b) Turbulent kinetic energy contour map

As shown in subgraph (a) of Figure 4, when wind blows from the bow at a speed of 4.5 m/s, parallel to the x-axis, the wind speed may vary due to the influence of the shape of the separator equipment and the chemical injection system equipment. After passing through the Process Treatment Zone I, the wind, influenced by the height differences of the upper module equipment, forms two different movement trajectories at the junction of the Process Treatment Zone II. The crude oil metering skid on the starboard side is relatively high, causing the wind passing through the chemical injection system equipment to be blocked and recirculated, forming a relatively strong airflow between the chemical injection system and the crude oil metering skid with a wind speed of approximately 3.5 m/s. In contrast, the electrostatic dehydrator and the crude oil flash skid located behind the separator equipment are lower, allowing the wind to pass over the top with minimal impact, while a still air zone forms below due to the obstruction caused by

the separator, with a wind speed of about 0.2 m/s. After passing through the Process Treatment Zone II, the wind movement pattern is similar to the previous zone, with a stronger airflow forming between the main switch room and the power module, where the wind speed reaches approximately 5 m/s, while most other areas form still air zones.

Turbulent kinetic energy is a measure of turbulence intensity, with higher values indicating more intense turbulence. As shown in subgraph (b) of Figure 4, when the wind blows from the bow, large portions of the area become still air zones due to the blockage caused by the upper module equipment, with a turbulent kinetic energy k value of 0 $\mathrm{m}^2/\mathrm{s}^2$. In some areas, weak turbulence forms due to height differences between the equipment, where the turbulent kinetic energy k value ranges between 0.3 and 0.45 $\mathrm{m}^2/\mathrm{s}^2$. Additionally, in areas where the equipment is densely arranged, more significant turbulence is observed, with the turbulent kinetic energy reaching approximately 0.95 $\mathrm{m}^2/\mathrm{s}^2$ between the Process Treatment Zone I and the Process Treatment Zone II.

In summary, as the wind blows from the bow over the vessel, the arrangement of the upper module equipment causes the formation of still air and turbulence zones, providing conditions for the accumulation of combustible gas after a leak. The leaked combustible gas is not easily dispersed within a short period, and as the leakage duration increases, the formation of a combustible gas cloud that reaches the explosive limit becomes highly likely.

5.2.2 Diffusion field

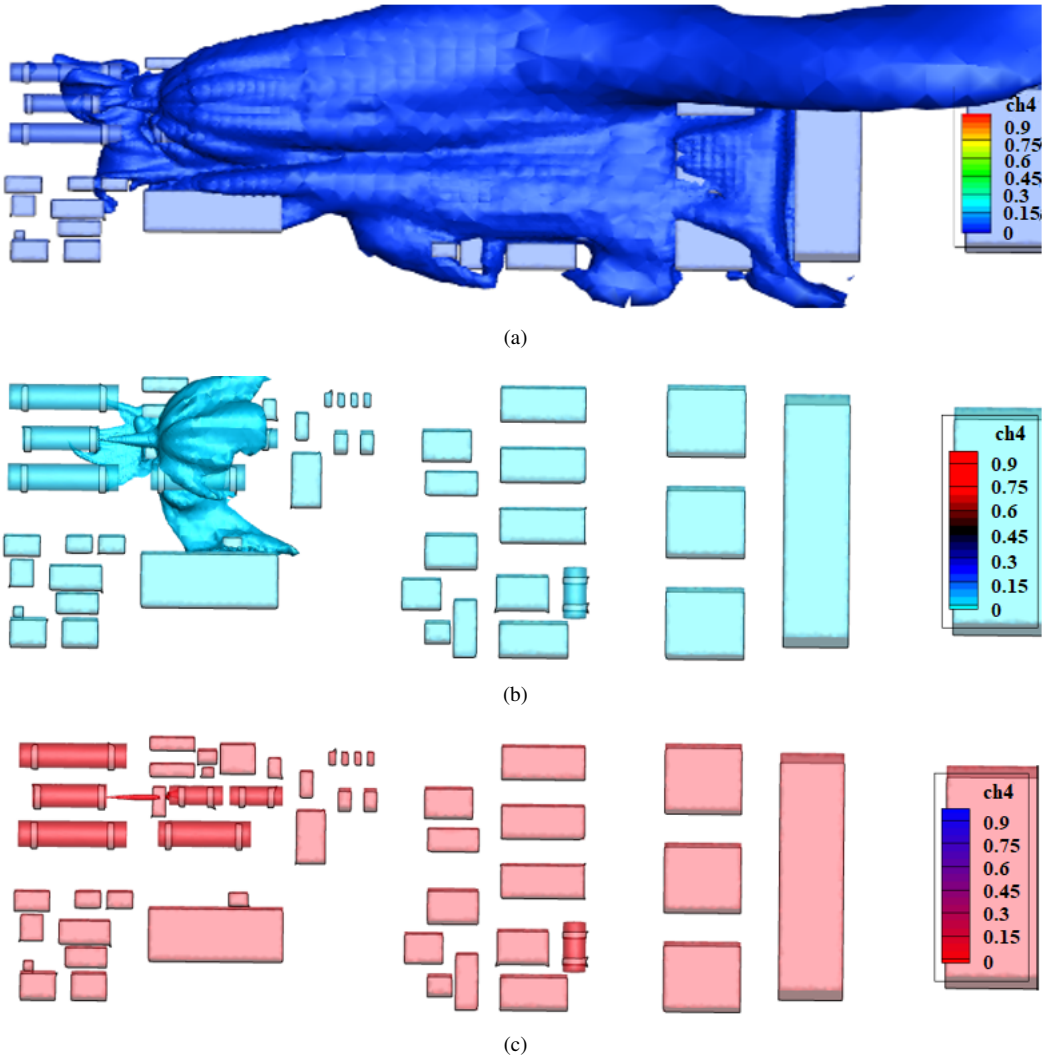

Figure 5. Diffusion concentration contour distribution map of the control group (a) 0.1%, (b) 1%, (c) 5%

Once the wind field was stabilised, the setting was changed from steady-state to transient. In the turbulence model, the buoyancy option was selected, and the non-reactive species transport model was activated. The fuel inlet was set to mass flow rate, with the rate defined as 5.188 kg/s. The methane composition was set to 100%, and the oxygen content at the air inlet was set to 0.23. The simulation time was set to 180 s. To intuitively observe the scale of methane leakage, methane concentration contour values of 0.1% (optimal diffusion effect), 1% (industrial natural gas

alarm level), and 5% (methane lower explosive limit) were chosen as criteria for determining the methane diffusion range. After processing the simulation results, the methane diffusion scale was obtained, as shown in Figure 5.

It is evident that gas with lower concentrations diffuses over a broader area. Influenced by the wind field, the leaked gas gradually tends to move toward the downwind equipment. When the gas is ejected at a high velocity, it is partially redirected upon encountering process equipment, dispersing in multiple directions. Although the natural wind helps disperse the accumulated methane, the turbulence generated by equipment obstructions facilitates the rapid concentration of methane in certain areas. While the 5% methane concentration isosurface can effectively represent the hazardous region of methane diffusion, its diffusion range changes little, making it less effective in reflecting the overall diffusion pattern of methane. The 1% methane concentration isosurface, on the other hand, meets industrial natural gas alarm requirements, covers a larger diffusion area, and can both represent the diffusion pattern of methane and indicate hazardous regions. Therefore, the 1% methane concentration isosurface was chosen as the primary subject for studying methane diffusion patterns.

The methane diffusion scale at a 1% concentration isosurface over various time points is shown in Figure 6. It is clear that during the first 30 s, the methane diffusion scale rapidly increases in all dimensions. Between 30 and 60 s, the longitudinal diffusion of methane slows due to the dense arrangement of equipment. From 60 s until the end of the diffusion process, methane diffusion stabilises, with the scale in all dimensions remaining relatively unchanged. The longitudinal diffusion scale of methane reaches 37 m, the lateral diffusion scale is 27 m, and the vertical diffusion scale is 10 m, covering an area of 999 m^2 with a volume of approximately 2997 m^3. At 180 s, when the leakage ends, the methane diffusion area reaches 962 m^2, with a volume of 2883 m^3.

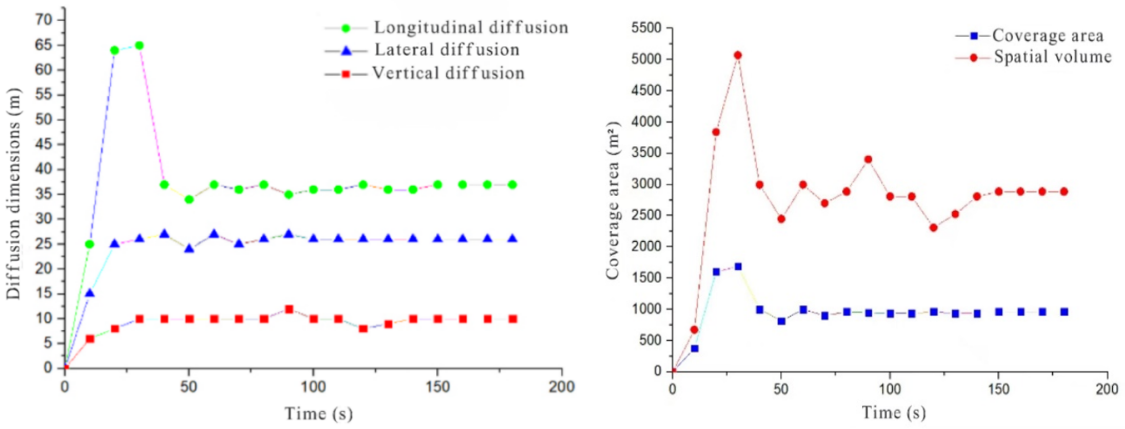

Figure 6. Methane diffusion scale of the control group

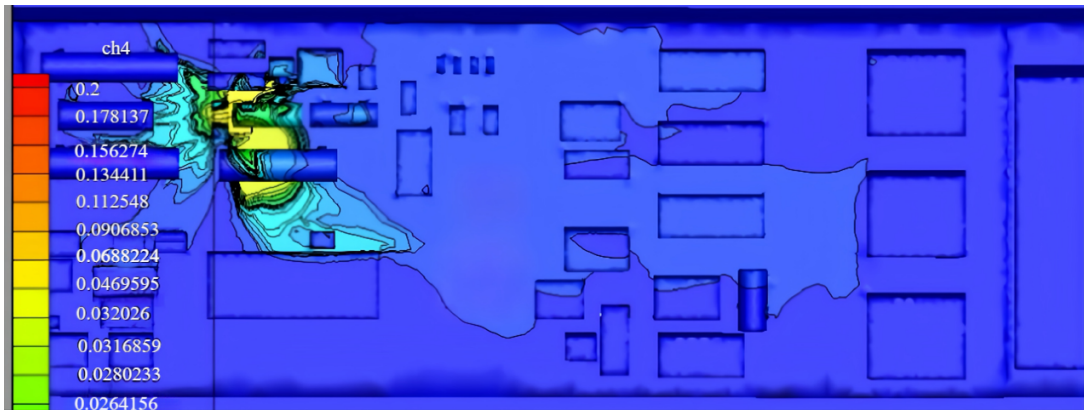

Figure 7. Distribution of methane leakage concentration at 180 s

5.2.3 Concentration field

Methane's explosive concentration range in air is between 5% and 15%. When methane concentration falls within this range, a vapor cloud explosion may occur if it encounters an ignition source. The dense arrangement of equipment in the upper module of the FPSO provides conditions for the accumulation of methane concentration after a leak. While natural wind can effectively disperse accumulated methane, turbulence caused by equipment obstructions

accelerates methane concentration in certain areas. The distribution of methane concentration in the FPSO upper module after the leak is shown in Figure 7.

As shown in Figure 7, after the leak has ended, large areas near the crude oil heat exchanger skid and the secondary heater skid have methane concentrations ranging between 6% and 9%, which fall within the explosive concentration range. Therefore, there is a possibility of a vapor cloud explosion occurring after the gas leakage in the FPSO upper module has been completed.

5.3 Characteristics of Gas Leakage Under Different Working Conditions

The literature indicates that wind direction, wind speed, and leakage aperture significantly influence the diffusion characteristics of combustible gas leakage. However, due to the complexity of the influencing mechanisms and the computational difficulty, few researchers have investigated the variations in gas leakage patterns in the upper module of the FPSO under combined working conditions. In this study, the method of orthogonal design was applied to simplify the complex combinations of working conditions into 16 typical conditions. A common working condition was selected as the control group. By comparing the simulation results, the influence of different factors on the diffusion characteristics of combustible gas leakage was explored.

5.3.1 Influence of wind speed

In the orthogonal design table, a leakage aperture of 40 mm, a wind speed of 0.5 m/s, and a headwind direction were selected, meaning the leakage aperture and wind direction remained unchanged while only the wind speed was varied. Working Condition 1 was chosen to explore the effect of wind speed on methane leakage diffusion.

The diffusion scale diagram of the 1% methane concentration isosurface is shown in Figure 8. By comparing Figure 6 and Figure 8, it is clear that wind speed significantly affects the methane diffusion process. The greater the wind speed, the further methane spreads in the direction of the wind. Under calm wind conditions, methane primarily diffuses vertically and towards the less obstructed port side. However, when there is a headwind, methane mainly spreads longitudinally along the vessel. On the other hand, while wind speed increases the diffusion scale of methane, it also accelerates its dilution. Wind speed plays a critical role in the dispersal of methane. Additionally, due to the reduced influence of natural wind, the trajectory of methane in the test group is freer, resulting in greater vertical and lateral diffusion compared to the control group. The coverage area and spatial volume formed are also significantly larger than those in the control group.

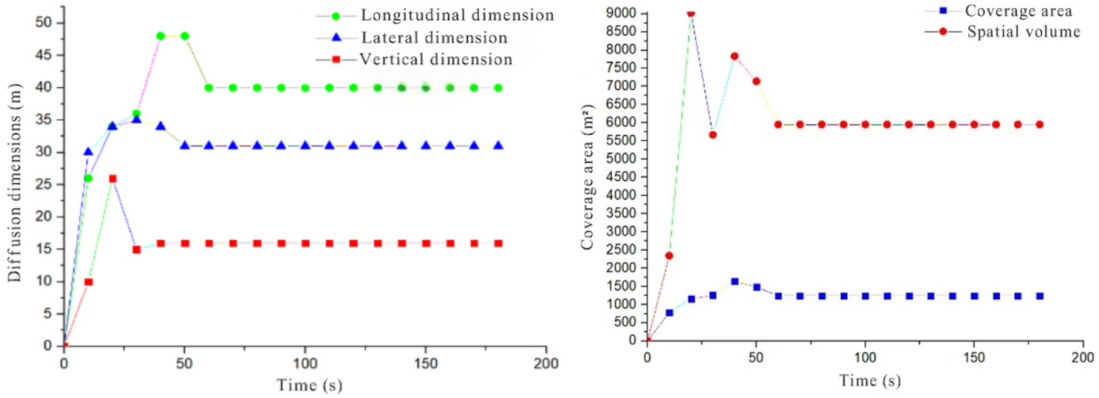

Figure 8. Methane diffusion scale diagram in Working Condition 1

From the analysis above, it is evident that wind speed has a significant impact on the diffusion of methane. Exploring the effect of wind speed on methane diffusion is of substantial practical importance.

5.3.2 Influence of wind direction

In the orthogonal design table, a leakage aperture of 40 mm and a wind speed of 4.5 m/s were selected, with the wind direction set as tailwind. In this scenario, the leakage aperture and wind speed remained unchanged, while the wind direction was varied to investigate the influence of wind direction on methane diffusion characteristics (Working Condition 6).

The 1% methane concentration isosurface was selected, and the methane diffusion scale data for different time intervals was post-processed. The resulting methane diffusion scale diagram is shown in Figure 9.

By comparing Figure 6 and Figure 9, it can be observed that the maximum longitudinal diffusion scale of methane in the control group is 65 m, which is greater than the 54 m observed in the test group. However, the maximum lateral diffusion scale of 31 m and the vertical diffusion scale of 15 m in the test group are higher than the control group's 27

m and 10 m, respectively. After the leakage is complete, the coverage area of methane in the control group is 962 m^2, while the test group's coverage area is approximately the same at 960 m^2. The spatial volume of methane in the control group is 2886 m^3, whereas the test group has a larger spatial volume of 4032 m^3.

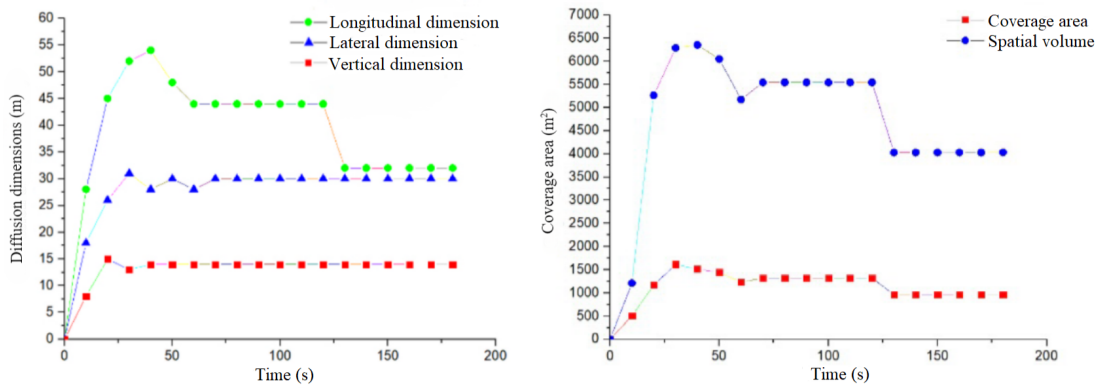

Figure 9. Methane diffusion scale diagram in Working Condition 6

From the above analysis, it is evident that wind direction can alter the process, scale, and mass of methane diffusion. Investigating the influence of wind direction as an influencing factor on methane diffusion is of great practical significance.

5.3.3 Influence of leakage aperture

In the orthogonal design table, a leakage aperture of 60 mm, a wind speed of 4.5 m/s, and a headwind direction were selected. In this scenario, the wind direction and wind speed remained unchanged, while only the leakage aperture was varied to investigate the influence of the leakage aperture on methane diffusion characteristics (Working Condition 2).

The 1% methane concentration isosurface was selected, and the methane diffusion scale data for different time intervals were post-processed. The resulting methane diffusion scale diagram is shown in Figure 10.

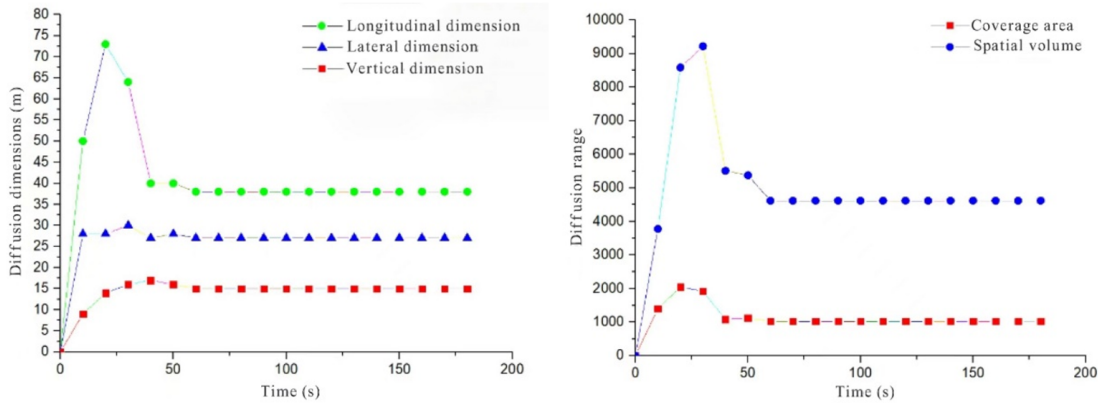

Figure 10. Methane diffusion dimensions in Working Condition 2

By comparing Figure 6 and Figure 10, it can be observed that an increase in aperture size significantly affects the methane leakage dimensions, particularly during the first 30 s. In the test group, the longitudinal dimension of methane reached 50 m after just 10 s, whereas it only reached 25 m in the control group. The test group achieved its maximum longitudinal diffusion size of 73 m within 20 s, while the control group reached a maximum longitudinal diffusion size of 65 m only after 30 s. After 30 s, the size and diffusion patterns between the control group and the test group show little difference, following a general trend of increase followed by decrease. After the leakage is complete, the methane coverage area in the control group was 962 m^2, while the test group's coverage area was slightly larger at 1026 m^2. The spatial volume of methane in the control group was 2886 m^3, whereas the test group had a significantly larger volume of 4617 m^3.

From the above analysis, it is clear that leakage aperture size has a significant impact on methane diffusion scale, making it practically meaningful to explore the influence of leakage aperture on methane diffusion characteristics.

5.3.4 Gas leakage characteristics with multiple influencing factors

The method of controlling variables can be used to explore how changes in a single influencing factor affect the methane gas leakage characteristics of the FPSO upper module. However, due to the complex working environment of the FPSO, gas leakage in the upper module is often caused by the simultaneous variation of multiple influencing factors, which may interact with each other. Therefore, building on the previous research, this section explores how multiple changing factors influence the leakage and diffusion characteristics of methane.

To investigate the effect of multiple influencing factors on the longitudinal diffusion of methane, the 1% methane concentration isosurface was selected. The longitudinal diffusion data for the 16 orthogonal design scenarios and one control condition were post-processed at various time intervals. The results are shown in Figure 11, illustrating the longitudinal diffusion time of methane under multiple working conditions. As can be seen from the figure, the longitudinal diffusion distance of most methane gas scenarios initially increases, then decreases, and finally stabilises. Comparatively, the maximum longitudinal diffusion distance for headwind and tailwind conditions is greater than that for port and starboard winds, with the primary effect of headwind and tailwind being an increase in methane concentration in the diffusion area. The methane leakage aperture and wind speed significantly affect the maximum longitudinal diffusion distance. When the leakage aperture is 100 mm and the headwind speed is 10 m/s, the maximum longitudinal diffusion distance of methane reaches 109 m.

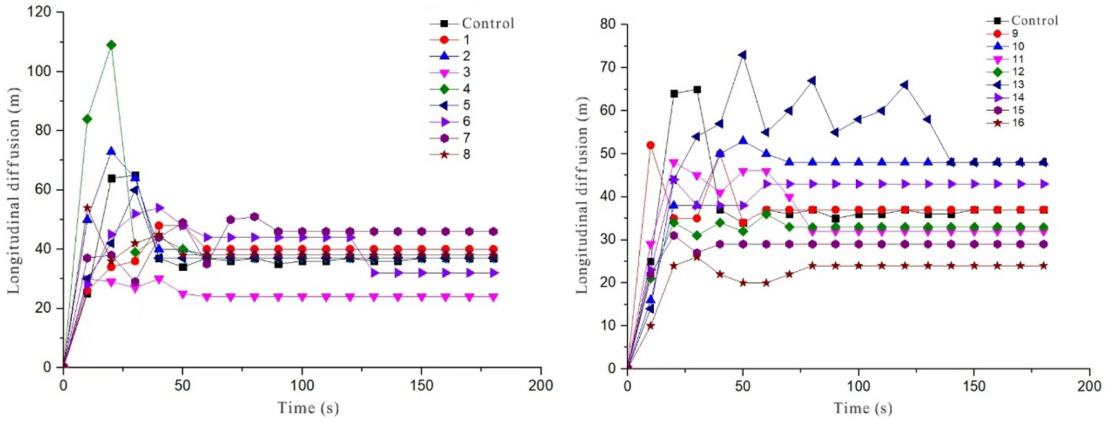

Figure 11. Longitudinal diffusion time of methane under multiple working conditions

To investigate the effect of multiple influencing factors on the transverse diffusion of methane, the 1% methane concentration isosurface was selected. The transverse diffusion data for the 16 orthogonal design scenarios and one control condition were post-processed at various time intervals. The resulting transverse diffusion time distribution of methane under multiple working conditions is shown in Figure 12.

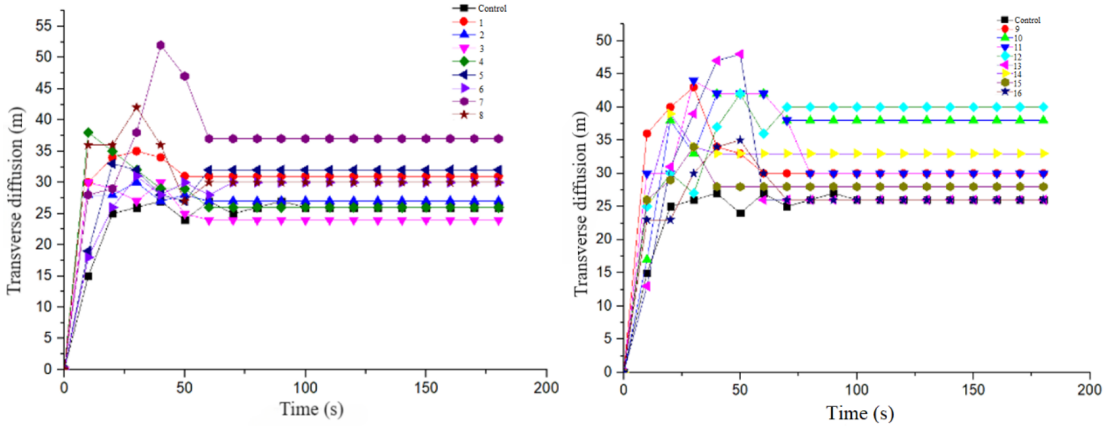

Figure 12. Transverse diffusion time distribution of methane under multiple working conditions

As shown in Figure 12, the transverse diffusion pattern of methane is similar to that of longitudinal diffusion, with most conditions showing an initial rapid increase followed by a decrease, ultimately stabilising. However, due to the greater longitudinal length of the FPSO compared to its transverse length, and the dense arrangement of longitudinal equipment near the leakage aperture in the upper module, the maximum transverse diffusion distance and the stabilised

methane diffusion distance are generally greater in the port and starboard wind conditions compared to headwind and tailwind conditions. When the leakage aperture is 100 mm and the tailwind speed is 8 m/s, the maximum transverse diffusion distance of methane reaches 52 m, the largest value among all orthogonal design conditions.

To investigate the effect of multiple influencing factors on the vertical diffusion of methane, the 1% methane concentration isosurface was selected. The vertical diffusion data for the 16 orthogonal design scenarios and one control condition were post-processed at various time intervals. The resulting vertical diffusion time distribution of methane under multiple working conditions is shown in Figure 13.

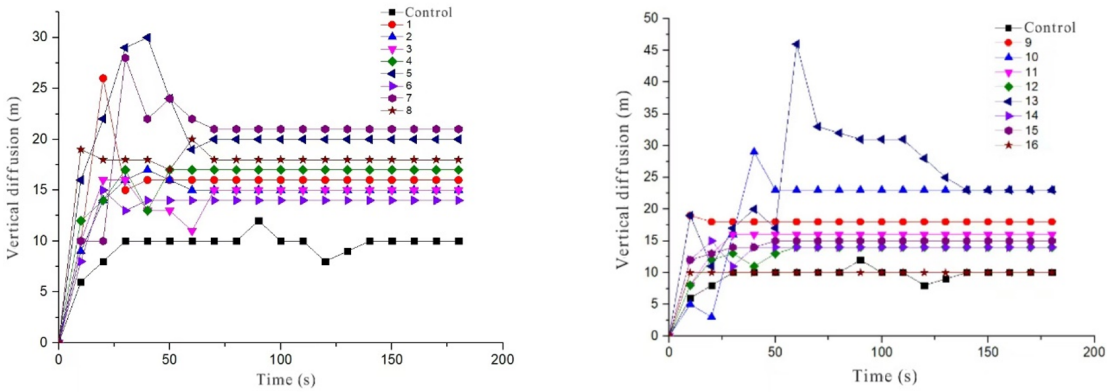

Figure 13. Vertical diffusion time distribution of methane under multiple working conditions

As shown in Figure 13, the vertical diffusion of methane does not exhibit as clear a pattern as its lateral and longitudinal diffusion. Due to the lack of influence from major factors, methane reaches stable vertical diffusion within a short time in conditions where interactions are not as intense. After stabilisation, methane's vertical diffusion is primarily driven by its own buoyancy, leading to lower vertical diffusion scales compared to lateral and longitudinal diffusion. When the leakage aperture is 100 mm and the starboard wind is 0.5 m/s, due to the low wind speed and large aperture, methane's diffusion trajectory is mostly governed by its own characteristics. During diffusion, methane predominantly spreads vertically upward due to surrounding obstacles, resulting in the vertical diffusion under this working condition reaching the maximum vertical diffusion scale of all scenarios at 46 m.

In summary, as observed from Figure 11, Figure 12, and Figure 13, the diffusion scale of methane across various dimensions is influenced by multiple interacting factors. The maximum longitudinal diffusion scale appears in Working Condition 4 at 109 m, the maximum lateral diffusion scale appears in Working Condition 7 at 52 m, and the maximum vertical diffusion scale occurs in Working Condition 13 at 46 m. These results suggest that methane diffusion exhibits diverse patterns under the influence of different factors. Therefore, it cannot be fully explained by the mechanism and outcomes of any single influencing factor.

6 Determination of the Most Hazardous Working Condition for Combustible Gas Leakage

Based on the analysis above, the determination of the most hazardous working condition for methane leakage cannot rely on the mechanism and outcomes of a single influencing factor. Therefore, building on the previous research, 16 orthogonal design scenarios and one control scenario were selected to consider the combined effects of multiple influencing factors. Methane diffusion mass and volume were chosen as the final evaluation indicators.

6.1 Determination of the Most Hazardous Working Condition Based on Diffusion Mass

Diffusion mass is one of the most direct indicators to measure the risk level of flammable gas leakage. The higher the methane diffusion mass within the explosion limit concentration range, the greater the risk of explosion caused by flammable gas leakage. In this study, the methane mass integral within the fluid domain was selected as the evaluation criterion. Through post-processing the methane diffusion mass integral over different time periods, the distribution of methane diffusion mass under multiple working conditions was obtained, as shown in Figure 14.

As shown in Figure 14, the methane diffusion mass under multiple working conditions exhibits a similar pattern. Except for Working Conditions 1, 5, 9, and 13, the methane diffusion mass initially grows at a constant rate, followed by a slight decrease before stabilising or continuing to grow slowly. This pattern occurs because, in the early stages of diffusion, methane primarily spreads within the fluid domain, with its concentration accumulating. During this period, the methane mass increases steadily due to the mass flow rate. After some time, a portion of the methane is carried outside the fluid domain due to external wind and its kinetic energy. At this point, the rate of methane dispersion exceeds the rate of accumulation, leading to a slight decrease in methane mass. Once diffusion stabilises, the methane concentration also stabilises or increases slowly. In Working Conditions 1, 5, 9, and 13, static wind

conditions prevent methane from diffusing out of the fluid domain within the leakage time. Therefore, methane diffusion mass continues to increase at the mass flow rate. Overall, after the leakage is complete, the condition with the largest methane diffusion mass is Working Conditions 13, with a diffusion mass of 3664 kg, indicating that the most hazardous working condition is when the leakage aperture is 100 mm and the starboard wind is 0.5 m/s.

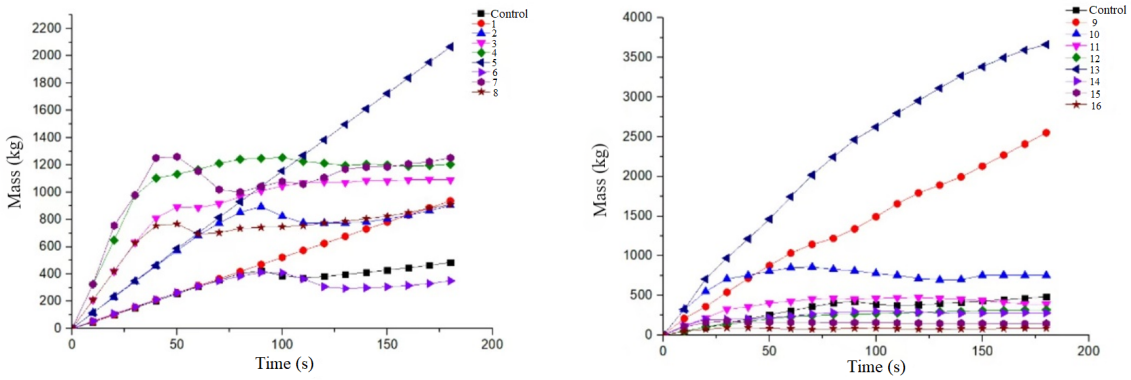

Figure 14. Time distribution of methane diffusion mass under multiple working conditions

6.2 Determination of the Most Hazardous Working Condition Based on Spatial Volume

The spatial volume of the flammable gas cloud is another critical indicator for assessing the risk level of methane leakage. The larger the volume of the flammable gas cloud within the explosion limit concentration range, the more severe the consequences of the flammable gas leakage. To maximise the consequences of methane leakage, the 1% concentration isosurface, corresponding to the industrial natural gas alarm concentration, was selected to calculate the spatial volume of the flammable gas cloud in this study. By post-processing the methane spatial volume data at different time intervals for each condition, the spatial volume and time distribution of methane under multiple working conditions were obtained, as shown in Figure 15. The spatial volume of methane generally follows a diffusion pattern of initial growth followed by stabilisation in most working conditions. However, since its variation is constrained by three dimensions, the diffusion pattern exhibits a more complex mechanism compared to that observed in a single dimension. Thus, measuring methane diffusion solely based on a single dimension does not provide a comprehensive understanding of the diffusion scale.

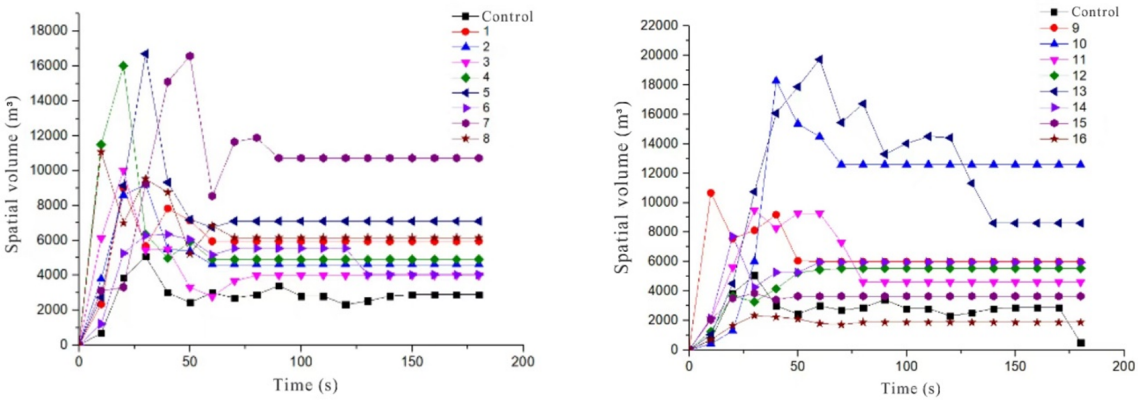

Figure 15. Time distribution of methane's spatial volume under multiple working conditions

After the methane leakage was complete, the maximum spatial volume occurred under Working Condition 10, reaching 12,585.6 m^3. When a wind speed of 4.5 m/s blew from the port side of the vessel, the dense equipment in the left half of the Industrial Processing Zone I blocked most of the incoming airflow. By the time the wind reached the vicinity of the leakage point, the wind speed diminished significantly, reducing to approximately 1.8 m/s. When the leakage aperture was 100 mm, the leakage rate reached 32.425 kg/s. The high-velocity methane stream, driven by the wind, primarily diffused toward the aft starboard side of the vessel. The dense equipment in Industrial Processing Zone II significantly slowed the dispersion of methane, resulting in a larger area with a 1% methane concentration compared to the scenario with wind from the bow. In contrast, when the wind came from the starboard side, the equipment density on the left side of Industrial Processing Zone II was considerably lower than on the right side,

leading to a much faster rate of methane dispersion compared to longitudinal winds. This resulted in a slightly smaller methane volume under starboard wind conditions.

6.3 Determination of the Most Hazardous Working Condition

Both diffusion mass and spatial volume can be used as evaluation indicators for hazardous methane leakage conditions. However, relying solely on diffusion mass as the final evaluation criterion may result in extreme conditions where the diffusion mass is large, but the volume is small. In such working conditions, the methane concentration could exceed the upper explosion limit, making it unreasonable to classify this as the most hazardous condition. Similarly, using only spatial volume as the final criterion could result in conditions where the volume is large, but the diffusion mass is small. In these working conditions, the methane concentration may fall below the lower explosion limit, making it equally unreasonable to consider this as the most hazardous condition. Therefore, this study integrates both diffusion mass and spatial volume as evaluation indicators. First, the five most hazardous conditions for both diffusion mass and spatial volume were selected. After removing duplicate conditions, the ratio of mass to volume was calculated as the evaluation criterion. This was compared with the explosion concentration to determine the most hazardous working condition for methane leakage.

According to Figure 14 and Figure 15, the five most hazardous working conditions based on methane diffusion mass and spatial volume are presented in Table 3.

Table 3. Dangerous working conditions of methane leakage based on diffusion mass and spatial volume

Name	1	2	3	4	5
Working condition number	13	9	5	7	4
Diffusion mass (kg)	3664	2551	2067	1254	1205
Working condition number	10	7	13	5	8
Spatial volume (m^3)	10977	9352	7511	6196	5369

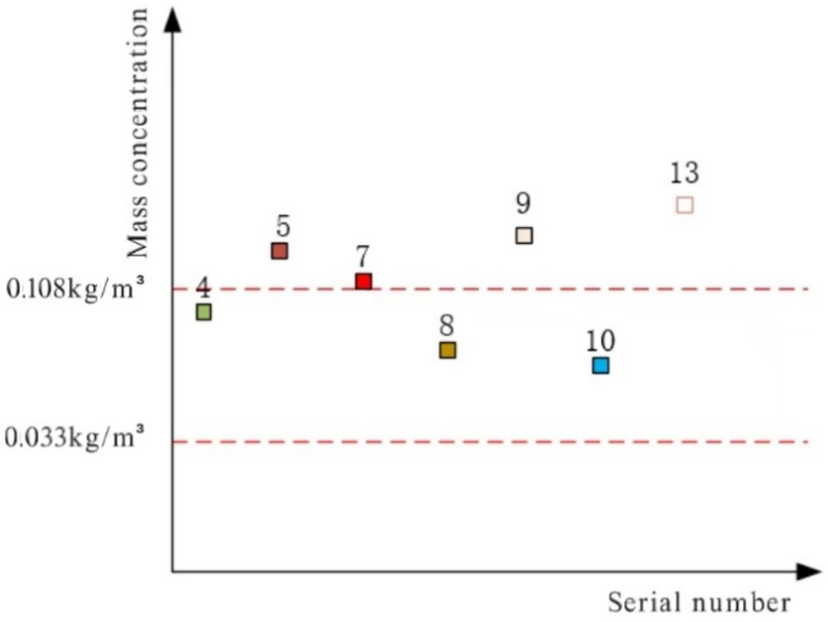

Figure 16. Evaluation of hazardous working conditions

As shown in Table 3, after eliminating the duplicate working conditions, a total of seven hazardous conditions remain: Working Conditions 4, 5, 7, 8, 9, 10, and 13. The calculated mass concentrations for these conditions are 0.282 kg/m³, 0.334 kg/m³, 0.134 kg/m³, 0.169 kg/m³, 0.488 kg/m³, 0.069 kg/m³, and 0.317 kg/m³, respectively. The methane diffusion mass data selected in this study represents the total methane mass within the entire fluid domain, while the methane spatial volume data corresponds to the methane volume at a concentration of 0.01. Therefore, the calculated results are likely higher than the actual methane mass concentrations. To provide a more accurate estimation of methane mass concentration, the maximum diffusion spatial volume was determined by selecting the maximum values for each dimension across all conditions after complete methane leakage. The maximum spatial

volume of methane was found to be 48 meters in length, 40 meters in width, and 23 meters in height. It was also assumed that the methane mass is uniformly distributed within this maximum diffusion region. After adjustment, the methane mass concentrations for the hazardous working conditions are 0.104 kg/m^3, 0.178 kg/m^3, 0.108 kg/m^3, 0.079 kg/m^3, 0.221 kg/m^3, 0.065 kg/m^3, and 0.317 kg/m^3, respectively. The explosion limit range for methane is between 5% and 15%, which corresponds to a mass concentration range of 0.035 kg/m^3 to 0.108 kg/m^3. Using methane explosion mass concentration as the evaluation criterion, the hazardous level of each condition can be determined by referring to the evaluation chart of hazardous working conditions shown in Figure 16.

As shown in Figure 16, Working Conditions 4, 8, and 10 all fall within the explosive limit concentration range. Among these, Working Condition 4 exhibits the highest mass concentration. Thus, it was selected as the most hazardous working condition. When the leakage aperture was set to 100 mm, the exit velocity reached 32.425 m/s. Methane, which moved forward with an initial kinetic energy, encountered a headwind with a velocity of 10 m/s. This high-concentration methane gas rapidly dispersed toward the stern and both sides of the vessel. Due to the influence of the upper module equipment, the dispersed methane could not be effectively evacuated in a short period, resulting in an accumulation of methane mass within the vessel. The volume of methane clouds within the explosive concentration range expanded continuously, making Working Condition 4 a potential candidate for the most hazardous condition.

Based on the two evaluation criteria, i.e., spatial volume and diffusion mass, using methane's explosive mass concentration as the standard, it was determined that the most hazardous working condition among the 17 research scenarios of methane leakage in the upper module of the FPSO is a leakage aperture of 100 mm, with a headwind direction at a velocity of 10 m/s. However, this wind speed is relatively high at 10 m/s. Based on earlier findings regarding the influence of wind speed on diffusion mass and spatial volume, there exists the potential for an even more hazardous working condition when the wind speed is reduced to 8 m/s. Therefore, an additional working condition was considered: a leakage aperture of 100 mm, a headwind direction, and a wind speed of 8 m/s. The resulting methane diffusion mass is 1254 kg, with a diffusion volume of 4500.83 m^3. Compared to Working Condition 4, although the diffusion mass is identical, the diffusion volume increases by nearly 300 m^3, making this working condition even more hazardous. Therefore, the most dangerous working condition is a leakage aperture of 100 mm with a headwind direction and a wind speed of 8 m/s.

7 Conclusion

In this study, a theoretical model for gas leakage in the upper module of FPSO was developed, and potential gas leakage working conditions were simulated based on actual working environments. By using FLUENT software, a simulation model was established to study the gas leakage patterns under different working conditions. The most hazardous leakage working condition for combustible gases in the upper module of the FPSO was identified. The following conclusions were drawn:

a) When analysing the influence of different factors on flammable gas leakage characteristics, orthogonal design can be applied based on the number and levels of factors, and a typical condition can be selected as a control. By using the method of controlling variables and comparison tests, the effects of various influencing factors on gas leakage characteristics can be determined.

b) Simulation results indicate that the density and shape of equipment in the upper module of the FPSO significantly affect the diffusion outcomes. In engineering practice, the risk of flammable gas accumulation can be effectively reduced by improving the arrangement and design of upper module equipment. After diffusion, high concentrations of combustible gases tend to accumulate near the crude oil heat exchanger skids in Industrial Processing Zone II. Since the leaked gas typically contains toxic gases such as H_2S, personnel should avoid this area during a leak.

c) In the studied working conditions, individual factors exert a significant impact on the characteristics of gas leakage. Wind speed primarily affects the gas leakage volume. When wind speed is below 8 m/s, it mainly promotes gas diffusion. However, when it exceeds 8 m/s, it predominantly facilitates dispersion. Leakage aperture significantly influences the diffusion mass, generally increasing with larger apertures. Wind direction can alter the diffusion trajectory of the gas. Due to the varying number and arrangement of equipment at different locations, wind direction indirectly affects the diffusion mass and volume.

d) The mechanism by which multiple factors influence gas leakage is complex. Overall, wind speed exerts the greatest influence on the longitudinal diffusion of gas compared to wind direction and leakage aperture. Wind direction, however, has a more pronounced effect on transverse diffusion, while leakage aperture has the most significant impact on vertical diffusion.

e) Based on the two evaluation criteria of spatial volume and diffusion mass, and in combination with the diffusion patterns of combustible gas leakage, the most hazardous condition was determined to involve a leakage aperture of 100 mm, a headwind direction, and a wind speed of 8 m/s.

Data Availability

The data used to support the findings of this study are available from the corresponding author upon request.

Conflicts of Interest

The authors declare no conflict of interest.

References

[1] L. K. Dasanayaka and P. D. Yapa, "Role of plume dynamics phase in a deepwater oil and gas release model," *J. Hydro-environ. Res.*, vol. 2, no. 4, pp. 243–253, 2009. https://doi.org/10.1016/j.jher.2009.01.004

[2] V. Pranesh, K. Palanichamy, O. Saidat, and N. Peter, "Lack of dynamic leadership skills and human failure contribution analysis to manage risk in deep water horizon oil platform," *Safety Sci.*, vol. 92, pp. 85–93, 2017. https://doi.org/10.1016/j.ssci.2016.09.013

[3] C. G. Ramsay, A. J. Bolsover, R. H. Jones, and W. G. Medland, "Quantitative risk assessment applied to offshore process installations. Challenges after the piper alpha disaster," *J. Loss Prev. Process Ind.*, vol. 7, no. 4, pp. 317–330, 1994. https://doi.org/10.1016/0950-4230(94)80045-6

[4] M. Kalantarnia, F. Khan, and K. Hawboldt, "Modelling of BP Texas City refinery accident using dynamic risk assessment approach," *Process Saf. Environ. Prot.*, vol. 88, no. 3, pp. 191–199, 2010. https://doi.org/10.1016/j.psep.2010.01.004

[5] L. Ottemöller and L. G. Evers, "Seismo-acoustic analysis of the Buncefield oil depot explosion in the UK, 2005 December 11," *Geophys. J. Int.*, vol. 172, no. 3, pp. 1123–1134, 2008. https://doi.org/10.1111/j.1365-246X.2007.03701.x

[6] D. Yang, G. Chen, J. Shi, and X. Li, "Effect of gas composition on dispersion characteristics of blowout gas on offshore platform," *Int. J. Nav. Archit. Ocean Eng.*, vol. 11, no. 2, pp. 914–922, 2019. https://doi.org/10.1016/j.ijnaoe.2019.02.009

[7] J. Cai, J. Wu, S. Yuan, D. Kong, and X. Zhang, "Prediction of gas leakage and dispersion in utility tunnels based on CFD-EnKF coupling model: A 3D full-scale application," *Sustain. Cities Soc.*, vol. 80, p. 103789, 2022. https://doi.org/10.1016/j.scs.2022.103789

[8] C. Chen, G. Reniers, and N. Khakzad, "A thorough classification and discussion of approaches for modeling and managing domino effects in the process industries," *Safety Sci.*, vol. 125, p. 104618, 2020. https://doi.org/10.1016/j.ssci.2020.104618

[9] J. H. Park, B. J. Kim, J. K. Seo, J. H. Park, J. S. Jeong, B. K. Oh, S. H. Kim, C. H. Park, J. K. Paik, and J. Czujko, "Load characteristics of steel and concrete tubular members under jet fire: An experimental and numerical study," in *29th International Conference on Ocean, Offshore and Arctic Engineering, Shanghai, China*, 2010, pp. 911–920. https://doi.org/10.1115/OMAE2010-20754

[10] B. J. Kim, J. Yoon, G. Yu, H. Ryu, Y. Ha, and J. K. Paik, "Heat flow analysis of an FPSO topside model with wind effect taken into account: A wind-tunnel test and CFD simulation," *Ocean Eng.*, vol. 38, no. 10, pp. 1130–1140, 2011. https://doi.org/10.1016/j.oceaneng.2011.05.004

[11] J. H. Kim, D. C. Kim, C. K. Kim, M. S. Islam, S. I. Park, and J. K. Paik, "A study on methods for fire load application with passive fire protection effects," *Ocean Eng.*, vol. 70, pp. 177–187, 2013. https://doi.org/10.1016/j.oceaneng.2013.05.017

[12] J. M. Sohn, S. J. Kim, B. H. Kim, and J. K. Paik, "Nonlinear structural consequence analysis of FPSO topside blastwalls," *Ocean Eng.*, vol. 60, pp. 149–162, 2013. https://doi.org/10.1016/j.oceaneng.2012.12.005

[13] K. Takahashi and K. Watanabe, "Advanced numerical simulation of gas explosion for assessing the safety of oil and gas plant," in *Numerical Simulations-Examples and Applications in Computational Fluid Dynamics*, 2010, pp. 377–388.

[14] S. Dan, C. J. Lee, J. Park, D. Shin, and E. S. Yoon, "Quantitative risk analysis of fire and explosion on the top-side LNG-liquefaction process of LNG-FPSO," *Process Saf. Environ. Prot.*, vol. 92, no. 5, pp. 430–441, 2014. https://doi.org/10.1016/j.psep.2014.04.011

[15] D. Yang, G. Chen, and Z. Dai, "Accident modeling of toxic gas-containing flammable gas release and explosion on an offshore platform," *J. Loss Prev. Process Ind.*, vol. 65, p. 104118, 2020. https://doi.org/10.1016/j.jlp.2020.104118

[16] J. Liu, J. Yu, H. Chen, Z. Yang, F. Kong, and Y. Lei, "Influence of arrangement modes of obstacles on vapor cloud explosion of offshore platform," *J. Safety Sci. Technol.*, vol. 15, no. 8, pp. 5–11, 2019. https://doi.org/10.11731/j.issn.1673-193x.2019.08.001

[17] H. Fang, H. Xue, and W. Tang, "Blast wave propagation characteristics in FPSO: Effect of cubical obstacles," *Ocean Eng.*, vol. 250, p. 111022, 2022. https://doi.org/10.1016/j.oceaneng.2022.111022

[18] K. Kang, X. Wang, J. Wang, W. Shi, Y. Sun, and M. Chen, "A critical review of a computational fluid dynamics (CFD)-Based explosion numerical analysis of offshore facilities," *Arch. Comput. Methods Eng.*, vol. 29, pp. 4851–4870, 2022. https://doi.org/10.1007/s11831-022-09756-1

[19] D. S. N. A. Shamsuddin, A. F. M. Fekeri, A. Muchtar, F. Khan, B. C. Khor, B. H. Lim, M. I. Rosli, and M. S. Takriff, "Computational fluid dynamics modelling approaches of gas explosion in the chemical process industry: A review," *Process Saf. Environ. Prot.*, vol. 170, pp. 112–138, 2023. https://doi.org/10.1016/j.psep.2022.11.090

[20] A. Qiao and S. Zhang, "Advanced CFD modeling on vapor dispersion and vapor cloud explosion," *J. Loss Prev. Process Ind.*, vol. 23, no. 6, pp. 843–848, 2010. https://doi.org/10.1016/j.jlp.2010.06.006

[21] S. M. Tauseef, D. Rashtchian, T. Abbasi, and S. A. Abbasi, "A method for simulation of vapour cloud explosions based on computational fluid dynamics (CFD)," *J. Loss Prev. Process Ind.*, vol. 24, no. 5, pp. 638–647, 2011. https://doi.org/10.1016/j.jlp.2011.05.007

[22] M. Saeed, J. Y. Yu, A. A. A. Abdalla, X. P. Zhong, and M. A. Ghazanfar, "An assessment of $\mathrm{k} - \varepsilon$ turbulence models for gas distribution analysis," *Nucl. Sci. Technol.*, vol. 28, pp. 1–8, 2017. https://doi.org/10.1007/s41365-017-0304-x

[23] J. K. Paik, J. Czujko, B. J. Kim, J. K. Seo, H. S. Ryu, Y. C. Ha, P. Janiszewski, and B. Musial, "Quantitative assessment of hydrocarbon explosion and fire risks in offshore installations," *Mar. Struct.*, vol. 24, no. 2, pp. 73–96, 2011. https://doi.org/10.1016/j.marstruc.2011.02.002